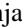



Experimental generation of coherent-state superpositions with a quantum memory

Viviane Cotte, Hector Simon, Benjamin Pointard , and Rosa Tualle-Brouri 
*Laboratoire Charles Fabry, Institut d'Optique Graduate School, CNRS, Université Paris-Saclay,
 2 Avenue Augustin Fresnel, 91127 Palaiseau, France*



(Received 15 July 2022; revised 26 September 2022; accepted 16 November 2022; published 8 December 2022)

We implement an iterative scheme for the generation of coherent states superpositions, using a quantum memory to take advantage of the iterative nature of the protocol. The generation rate has thus been increased by one order of magnitude, reaching 100 (Hz). Furthermore, the generated states were stored in the quantum memory during 184 (ns) before their characterization, paving the way toward the implementation of more complex iterative protocols.

DOI: [10.1103/PhysRevResearch.4.043170](https://doi.org/10.1103/PhysRevResearch.4.043170)

I. INTRODUCTION

Coherent state superpositions (CSSs) are nonclassical states that can be represented as superpositions $|\alpha\rangle \pm |-\alpha\rangle$ of two coherent states of amplitude $\pm\alpha$. Those states open a wealth of possible applications in quantum technologies. They are, among others, interesting for quantum communication [1–4], quantum computation, quantum error correcting codes, [5–9] and even metrology [10–12]. The availability of fast and efficient sources of CSS constitutes a major bottleneck in this perspective.

Since the first theoretical proposal for CSS generation with third-order nonlinear effect in a crystal [13], many experiments have produced optical CSSs in various ways: with heralding by photon detection events and/or homodyne conditioning [14–19], that includes iterative schemes [15,19], with superconducting microwave resonators [20,21] or in an optical cavity driven by a single atom [22], and more recently with high harmonic generation [23]. All of those methods have their advantages and drawbacks. CSSs in superconducting resonators can be produced efficiently with a large number of photons (up to 100) [21] but are trapped and therefore cannot be used for communication protocols, including data transmission in a scalable quantum computer. On the other hand, free propagating CSSs can be easily produced with heralding methods but the generation rate quickly decreases with the amplitude of the targeted CSS: A few groups have managed to exceed 100 (Hz) [18,22], however, typical emission rates for medium-size ($\alpha \approx 1.6$) free-propagating CSSs are usually of the order of the Hertz [14,16,17,19].

Iterative generation protocols [5,9,24,25], based on the possibility to increase CSS amplitude by merging CSSs of

lower amplitudes, could avoid the use of rare resources as Fock states with large photon numbers, and could even be initiated by single-photon states [19]. These protocols could be highly efficient through the storage of intermediate states in quantum memories [9]. However, despite recent progress of quantum memories in the continuous variable regime [26–29], the relevance of these protocols for CSS generation still needed an experimental assessment. We present here an implementation of such a protocol, with the capture and storage of intermediate resources before the required quantum operations and measurements. In this experiment, the quantum memory allows an improvement of the generation rate by a factor ≈ 10 , so rates of several kilohertz could be easily considered in the near future. Furthermore, the CSS generated in this experiment is stored during 184 (ns) in the quantum memory while maintaining its nonclassical nature, with negative values in its Wigner function. This paves the way toward the implementation of further iteration steps.

II. EXPERIMENTAL SETUP

The experiment consists of four main parts: a single photon source, an optical quantum memory, a homodyne detection system, and a phase measurement path (Fig. 1).

It begins with the generation of single photons pairs. We use a 850 (nm) pulsed (4.2 ps) Ti-Sa laser (Mira 900-D) operating at $f_{\text{TiSa}} = 76$ (MHz), part of which is exalted in a first synchronized cavity for second harmonic generation with a BiB_3O_6 crystal (BiBO) [30]. The resulting 425 (nm) pulse is sent in a second cavity for the generation of single photon pairs at 850 (nm) by spontaneous parametric down-conversion in a second BiBO crystal [31].

One of the photons is spatially and spectrally filtered using an optical fiber, a diffraction grating, and a slit before reaching an avalanche photodiode (APD, Perkin-Elmer-SPCM-AQR-13). Its detection heralds the presence of the other single photon by sending an electronic signal to all the devices that will control this second photon. With this system, we have an 850 (nm) heralded single photon source with an emission

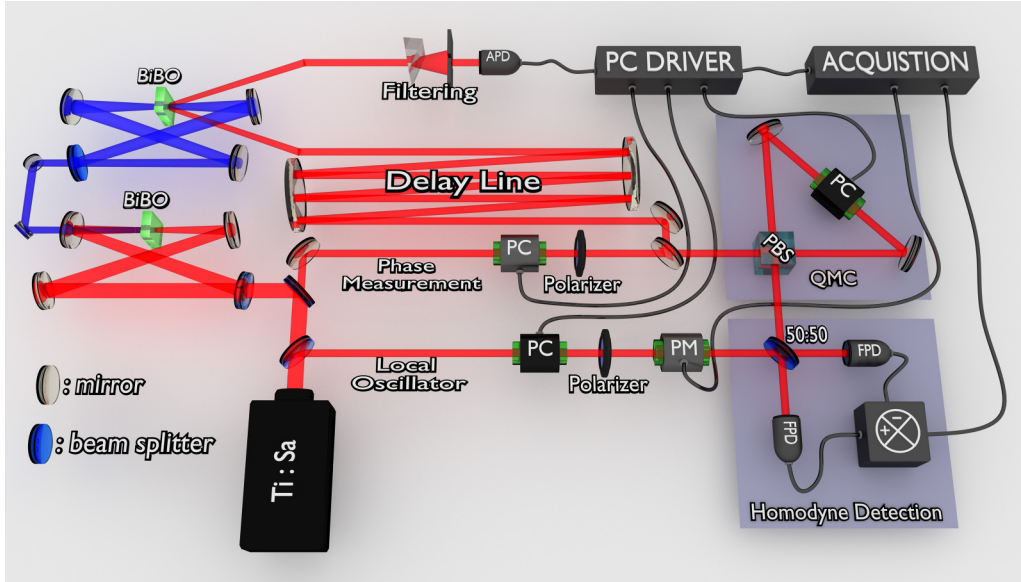


FIG. 1. Experimental setup. The main light source is a Ti-Sa picosecond laser. Part of the beam is frequency doubled in a first cavity to pump the production of photon pairs in a second cavity. The detection of one photon of the pair heralds the generation of the other one. The latter is delayed before entering in a third cavity which plays the role of a quantum memory (QMC). All the cavities are synchronized with the laser repetition rate. Pockels cells allow us to manage the pulses in real time. The signal at the output of the QMC is measured by homodyne detection. Parts of the laser beam are allocated to the local oscillator and to phase measurements.

rate $f_{|1\rangle} \approx 200$ (kHz) [31], corresponding to a probability of generating a single photon $P_{|1\rangle} = f_{|1\rangle}/f_{\text{TiSa}} \approx 0.25\%$.

The heralded photon is first sent through a 60 meter free-space optical line [32], while the APD electronic triggers the required control devices. Then this photon arrives in the quantum memory cavity (QMC), which includes a Pockels cell (PC) and a polarizing beam splitter (PBS) to store optical states [29] and realize other kinds of operations. The QMC is a low-loss optical cavity synchronized with the laser source, so at each round trip the stored state will exactly match the next emitted photon, if any. Likewise, the state released by the QMC will exactly match the local oscillator and can therefore be measured with a homodyne detection system [33].

A last path enables us to measure the phase shifts in the system by sending upon request attenuated coherent states toward the QMC from the back of a mirror (Fig. 1) (see Sec. III B).

The CSS generation is done in the QMC by sending a looping electronic sequence to the PC using fast programmable delay generators (BME-SG08p) triggered by the APD electronic signal and synchronized with the picosecond laser source. The sequence works as follow:

(i) We store a first photon in the QMC by flipping its polarization from horizontal (H) to vertical (V) with the PC ($\lambda/2$ operation).

(ii) When a second photon arrives in the QMC, the two photons constitute a $|1_H\rangle|1_V\rangle$ state. We then perform a $\lambda/4$ operation with the PC to get a superposition of two photons with opposite circular polarizations $|1_R\rangle|1_L\rangle$.

(iii) With such circular polarizations, the PBS acts on the photons as a symmetric beam splitter. One output port of this device is directed toward the homodyne detection to perform a projective quadrature measurement while the other one is stored in the QMC. If the homodyne measurement leads to a

quadrature near $X = 0$, the state in the cavity is projected onto

$$|\Psi_{\text{CSS}}\rangle = \frac{1}{\sqrt{3}}|0\rangle + \frac{\sqrt{2}}{\sqrt{3}}|2\rangle. \quad (1)$$

This final state has a 99% fidelity with a CSS of amplitude $\alpha = 1.63$ and a squeezing factor $s = 1.52$ [19].

(iv) The created state stays 14 round trips (184 ns) in the QMC before it is released ($\lambda/2$ with the PC) and measured with the homodyne detection.

This sequence is followed by a phase measurement sequence during which we send two coherent states that stay, respectively, 1 and 15 round trips inside the QMC, as detailed in Sec. III B. Let us stress that the storage time at step 4 of the sequence is arbitrary, and we could even wait for another photon to generate a three-photon CSS in a way very similar to steps 2 and 3 [9], as expected from an iterative protocol. Considering the storage time addressed in the present work (14 round trips), the QMC would allow an additional increase by a factor ≈ 14 of the generation rate for such a two-step generation protocol compared to a two-step protocol without QMC. The main difficulty to achieve this target is to control the phase of the local oscillator in real time.

The implementation of this sequence requires different technical skills (ability to switch from a $\lambda/2$ to a $\lambda/4$ operation on demand and in real time, ability to monitor the phase-shift induced by the QMC, and to control the storage time of the first photon...) that are the object of the next section.

III. IMPLEMENTATION OF THE ITERATIVE PROTOCOL

A. Control of the fast Pockels cells with PCI BMESG08p

To perform $\lambda/2$ and $\lambda/4$ operations, we use a fast Raicol PC, consisting of two RTP crystals. Its transmission loss is

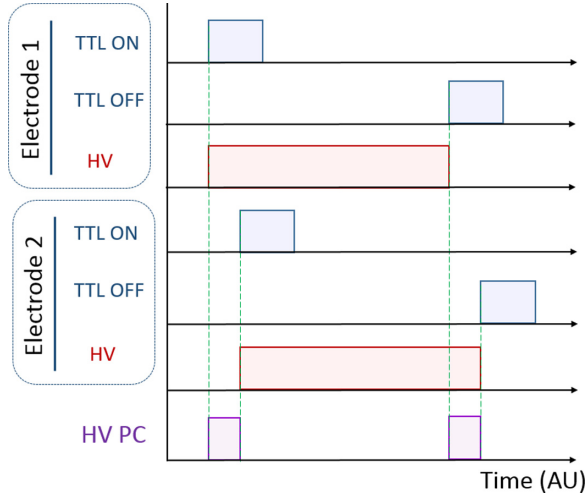


FIG. 2. Chronogram of the different signals sent to the PC of the QMC to make two HV $\lambda/2$ pulses.

theoretically lower than 0.4%, with a capacitance low enough (4 pF) to reach a rise/fall time below 10 (ns). Because of this fast transition time, the high voltage (HV) level cannot be adjusted in real time and is therefore fixed at a V_π level which is the voltage for $\lambda/2$ operations. Such operations are used for the storage and release of a light pulse, and this requires a short HV pulse on the PC to reach V_π for a specific pulse, without perturbation on the neighboring pulses. As the duration between two pulses is ≈ 13 (ns), the duration of this pulse therefore has to be lower than 26 (ns). A TTL pulse is sent to switch on a first electrode of the PC, then 13 (ns) later a second TTL pulse is sent to switch on the second electrode. This induces a V_π HV pulse between both electrodes (Fig. 2). TTL pulses are sent with a PCI card [BMESG08p] and have an arrival accuracy of 25 (ps).

In the procedure above, the delay between the TTL pulses is large enough for the voltage between both electrodes to reach V_π . With a reduced delay, this voltage could reach any value between 0 and V_π , so an accurate control of this delay allows us to deliver a programmable HV pulse. With this method, we can make any kind of V pulses, including the value $V_{\pi/2}$ required for $\lambda/4$ operations, by choosing the right timing. The quality of the $\lambda/4$ operation can be assessed through the measurement, after the PC, of the output ellipticity of a linearly polarized input pulse, which is of $44_{-2}^{+1^\circ}$ for the $\lambda/4$ delay (Fig. 3).

B. Phase measurement

Between each CSS sequence, there is a phase measurement sequence. We need to know the phase θ_{CSS} between the conditioning and our CSS measurement to reconstruct the Wigner function of our CSS by tomography [34,35]. This phase is the phase θ_s induced by the storage of 14 round trips in the QMC, up to a potential phase shift θ_0 related to residual birefringence in the $\lambda/4$ operation. We will write $\theta_{\text{CSS}} = \theta_s - \theta_0$ and $\theta_s = 14\theta_{\text{QMC}}$, where θ_{QMC} is the phase shift induced by one round trip in the QMC. We measure this phase by sending two attenuated coherent states in the QMC through the back of a mirror. Those two states stay, respectively, 1 and 15 round

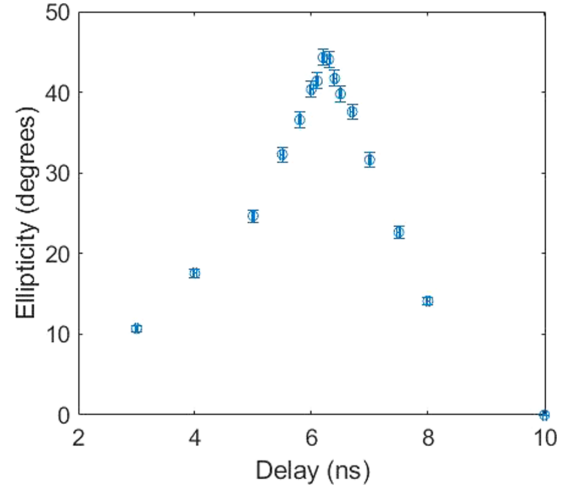


FIG. 3. Output ellipticity, after the PC, of a linearly polarized input pulse depending on the delay between the TTL pulses; ellipticity of a perfect circular polarization is 45° .

trips inside the QMC. If θ_N is the phase acquired by a coherent state after N round trips in the QMC, a subsequent homodyne measurement should give us access to the phases:

$$\theta_N - \theta_{OL} = \theta_1 + (N - 1)\theta_{\text{QMC}} - \theta_{OL},$$

where θ_{OL} is the phase of the local oscillator and θ_1 is the phase acquired by the coherent state for $N = 1$. Here one homodyne measurement is performed for each coherent state, at $N = 1$ and $N = 15$ round trips, and we assume that between the two measurements, separated by a few hundreds of nanoseconds, all phase variations are negligible. Thus, if we subtract the two phases, we get $\theta_s = 14\theta_{\text{QMC}}$.

Now, we just need to extract the phase from the homodyne measurements of the coherent states. To do so, we have installed a phase modulator that periodically adds (5 kHz) a $\pi/2$ phase shift to the local oscillator. Thus, we have access alternately to the sine and the cosine of the coherent states' phase [see Figs. 4(a)–4(c)]. By interpolating these cosine and sine measurements [Fig. 4(d)], we extract the phase [Fig. 4(e)].

This phase measurement can be counterchecked with NOON states of the form $(|01\rangle + e^{i\theta_{\text{CSS}}} |10\rangle)/\sqrt{2}$. Those NOON states can be generated by using the same protocol as for CSS, but without the first step storage of the first photon in the QMC. We can plot the correlation between both measurements after the $\lambda/4$ operation (x) and after the 14 round trips storage in the QMC (x') as a function of the measured phase θ_s ,

$$\langle xx' \rangle = \frac{\eta F (1 - p)^N}{2} \cos(\theta_s - \theta_0),$$

with F the fidelity of the single photons, p the losses per round trip in the QMC, and η the efficiency of the HD. The data are consistent with the theoretical model (see the Appendix) for typical values of $F \approx 0.82$, $\eta \approx 0.75$, $p \approx 0.009$, with a very low value of $\theta_0 \approx 4.8^\circ$, and thus endorse the phase measurement method [see Fig. 4(f)].

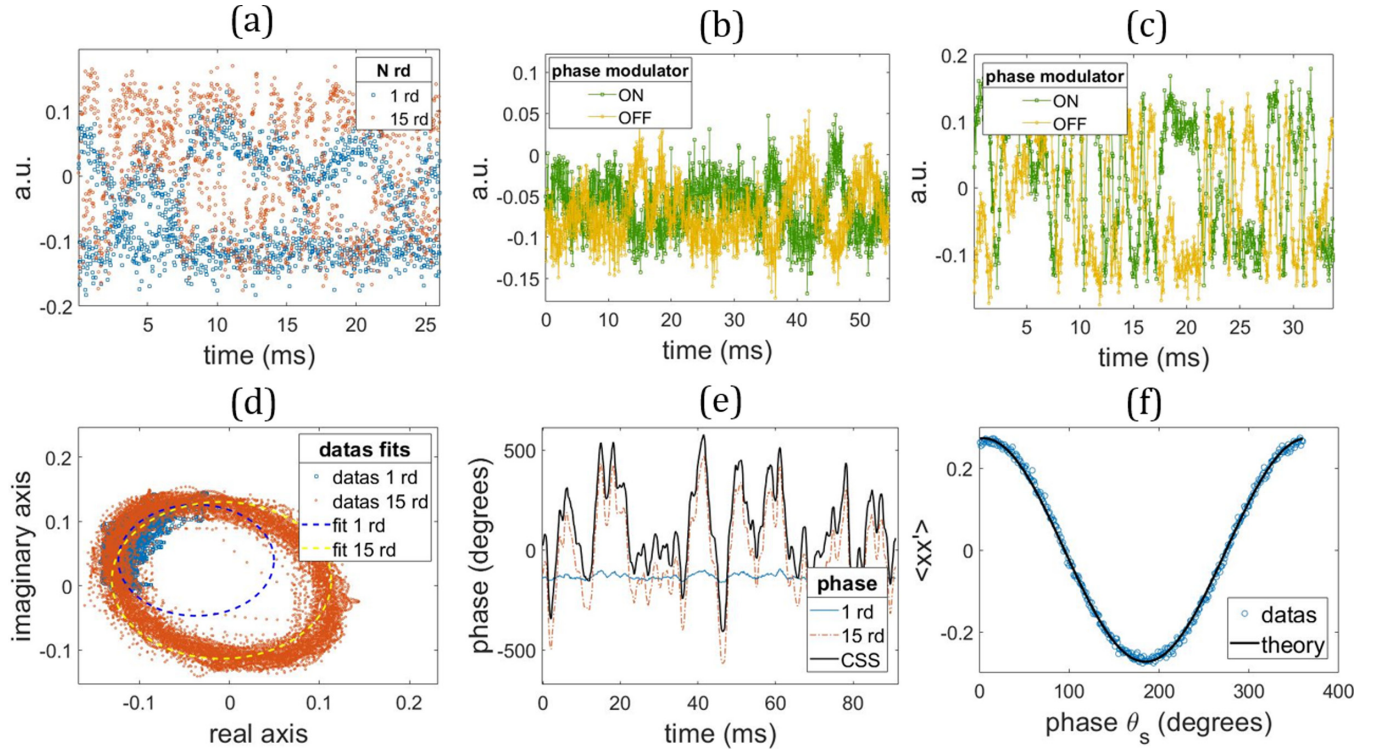


FIG. 4. (a) Signal on the HD of the two coherent states stored 1 and 15 round trips in the QMC. (b), (c) Signal of the coherent state stored 1 (b)/15 (c) round trip(s) with an extraction of the sine and cosine parts depending on the on/off status of the phase modulator. (d) Same as (b) and (c), but pictured in the complex plane, and with the fit used for phase extraction. (e) Extracted phase induces by the QMC for 1 round trip, 15 round trips, and their subtraction (CSS phase). (f) Correlation $\langle xx' \rangle$ of a NOON state: theoretical plot with $F = 0.82$, $\eta = 0.75$, $p = 0.009$, $\theta_s = 4.8^\circ$.

C. Control of the storage time

The storage time of the first photon inside the QMC is a major factor impacting both the quality and the generation rate of the generated CSS. The simulations in Fig. 5 present

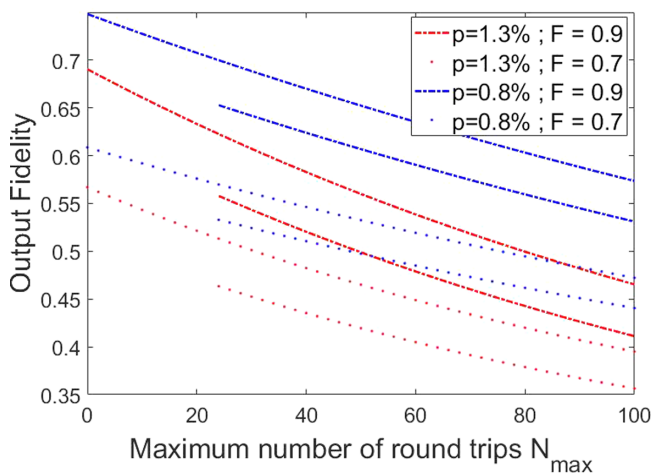


FIG. 5. Simulation of the fidelity to $|\psi_{\text{CSS}}\rangle$ of a CSS generated by the proposed protocol and stored in the QMC, depending on the maximum storage time N_{max} of the first photon in the QMC. Two values for the minimum storage time N_{min} are considered here (1 and 24 round trips, see main text), and the corresponding curves can be recognized from their starting point, as $N_{\text{max}} \geq N_{\text{min}}$.

the effect of the first photon's storage time on the output state fidelity to the target $|\Psi_{\text{CSS}}\rangle$ for different values of the fidelity F of initial photons and of the losses per round trip p in the QMC that are around our typical experimental values (losses $p \approx 1\%$, fidelity $F \approx 0.8$). Here, the simulation doesn't take into account some parasitic effects, like the phase uncertainty that is of ± 12 degrees and lowers the experimental fidelity of about 2.5% (see the Appendix). This figure clearly shows the decrease of the output state fidelity with the number of round trips in the QMC, which directly corresponds to the storage time. On the other hand, the CSS generation rate increases with the round trip number. CSS sequences are triggered by the generation of a first photon (stored in the QMC), and their success probability P_{CSS} depends on three major factors: the probability P_c to measure a quadrature around $X = 0$, the number of round trips N_{rt} for which a combination with the second photon can be considered, and the probability to generate a single photon $P_{|1\rangle}$:

$$P_{\text{CSS}} = P_c [1 - (1 - P_{|1\rangle})^{N_{\text{rt}}}] \approx P_c P_{|1\rangle} N_{\text{rt}}. \quad (2)$$

The success probability, and therefore the generation rate, thus linearly increases with the number of round trips in the cavity, and a compromise has to be found between fidelity and generation rate. To keep negative values for the Wigner function of the output state, we choose to limit this number to $N_{\text{max}} = 32$ round trips (421 ns).

In the present configuration of our experiment, electronic constraints prevent us from directly accessing the photon

storage time. To fix experimentally this value N_{\max} , we send a TTL pulse with duration $T = 120$ (ns) when this first photon is stored. This TTL pulse is delayed by $\tau = 310$ (ns) before reaching the acquisition card. If the conditioning of the CSS occurs between τ and $T + \tau$, we measure a positive TTL pulse. If the conditioning occurs after this time, we measure 0. This technique allows us to postselect all measurements with a first photon stored between τ and $T + \tau$, which corresponds to $N_{\min} = 24$ and $N_{\max} = 32$ round trips.

There is, therefore, also a minimum storage time N_{\min} of 24 round trips (315 ns). We thus have $N_{\text{rt}} = N_{\max} - N_{\min} + 1 = 9$ in the present experiment. This will lead to an increase of the success rate by about one order of magnitude.

By choosing to postselect events whose homodyne conditioning satisfies $|X| < 0.2$, we keep around $P_c \approx 13\%$ of our acquisitions without notable deterioration of the final state. The frequency generation of single photons $f_{|1\rangle}$ varies between 150 and 250 (kHz), and the CSS sequence is repeated at a $f_{|1\rangle}/3$ rate, as three sequences of the protocol are triggered by photon detection events (the storage of the first photon, the generation of the CSS, and the phase measurement sequence). Let us note that this reduction by a factor 3, as the relatively high value for N_{\min} , which leads to another reduction by a factor 3, are only linked to technical constraints in our setup. Such constraints could be removed through the development of more specific controllers, as planned in the near future. Taking all these constraints into account, we can expect from Eq. (2) a final generation rate of the CSS ranging from 100 to 300 (Hz) in the present experiment.

D. Tomography of CSS

We made different successful runs of measurements with CSS generation rates from 90 to 230 (Hz) and a negativity between -0.034 and -0.013 , depending on daily alignments. The results we present here have an uncorrected fidelity of $38.6^{+0.9}_{-1.9}\%$, and a corrected fidelity of $47.1^{+1}_{-3.8}\%$ with a negativity of $-0.0285^{+0.0113}_{-0.0175}$, for a generation rate of 100 (Hz) (single photon rate around 150 kHz). The corrected fidelity takes into account the 94% detection efficiency of the photodiodes and the overlapping of 90% between the mode of the local oscillator and the generated state, estimated from the interferences between the local oscillator and a probe beam injected in the optical parametric amplifier used for the emission of photon pairs [36]. It gives a correction factor of 0.76 ± 0.03 . We estimated uncertainties by drawing quadratures numerically with the same distribution (in number and average value) as experimental measurements [34].

We see in Fig. 6 the reconstructed Wigner function of our states. We can clearly see the two red bumps that represent the coherent states $|\alpha\rangle$ and $|\alpha\rangle$ as well as the interferences in the middle with a negative part in dark blue.

IV. CONCLUSION

In conclusion, we presented an experimental demonstration of an increase of the CSS generation rate using a quantum memory in an iterative protocol. A generation rate of almost 100 (Hz) has been achieved, which is among the highest values for such states in free space. Let us recall that the

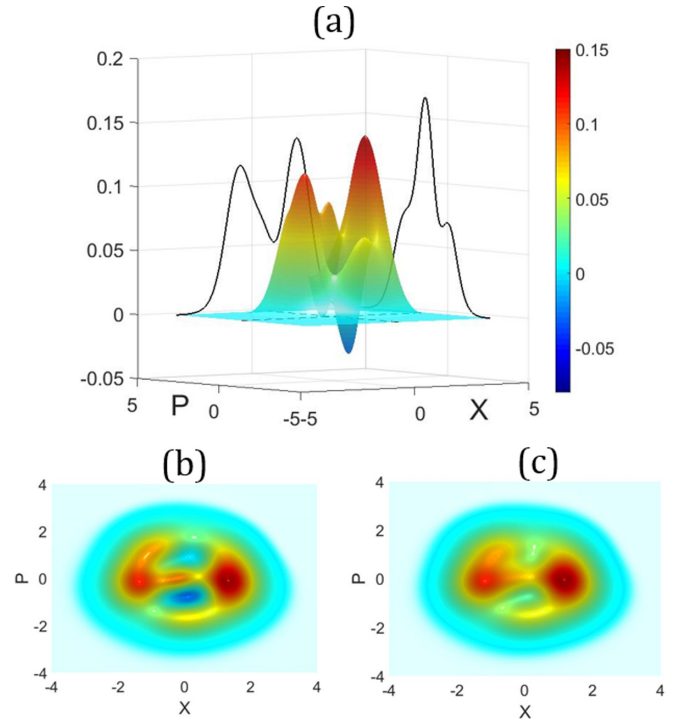


FIG. 6. (a) Wigner function of the corrected CSS. (b) Top view of the Wigner function of the corrected CSS. (c) Top view of the Wigner function of the uncorrected CSS.

experiment is still limited by electronic control systems, and a further increase by a factor of 9 can be expected through the development of dedicated electronics. Furthermore, a gain in the single-photon emission rate could be expected with more efficient photon detectors [18] or through the removal of the spatio-spectral filtering system through an engineering of the parametric amplification [37]. As the CSS emission rate depends quadratically on the single-photon rate, any improvement of the latter will have a huge incidence on the CSS rate, so rates of several kilohertz could be considered in the near future with such a setup. Furthermore, the CSSs are stored in the quantum memory during 184 (ns) before their characterization, and still present negative values of their corrected Wigner function. This setup therefore has the ability to implement further iteration steps, allowing further growth of the stored CSS by photon addition using the same protocol [9]. This technology paves the way toward the implementation of more complex protocols, using CSS as a basic resource.

ACKNOWLEDGMENTS

The authors thank Thorald Bergmann from Bergmann Messgeraete Entwicklung KG for his help with the control of the PCI BMESG08p. This work was supported by the Agence Nationale de la Recherche with the IGNITION project (Grant No. ANR-21-CE47-0015-01) and the SPOCQ project (Grant No. ANR-14-CE32-0019-01) and by the Région Ile-de-France DIM SIRTEQ (NewPaQC project).

APPENDIX: ANALYTICAL MODEL OF THE EXPERIMENT

This Appendix describes the analytical model that we use to predict the expected results (density matrix, fidelity, negativity...) for the CSS, knowing:

- (i) The experimental density matrix [31] of our single photon states before the QMC : ρ_{in} .
- (ii) The losses per round trip inside the QMC: p .
- (iii) The number of storage round trips inside the QMC for both the first single photon and the CSS.

A first photon arrives and is stored between N_{Imin} and N_{Imax} round trips inside the QMC. The probability distribution of the storage time N_1 , which depends on the arrival of a second photon, tends to a uniform distribution at low values of the probability $P_{|1\rangle}$ to generate a single photon. The simulations presented in this paper are performed in this limit, which is quite reasonable considering the low values of $P_{|1\rangle}$ in the experiment, in the range of a few per thousand. This approximation slightly underestimates the fidelities in Fig. 5, as it overestimates the probability to have high values of N_1 . The total losses for each equiprobable storage time $N_{\text{Imin}} < N_1 < N_{\text{Imax}}$ can be modeled by mixing the input state (mode 1) with a vacuum state (mode 2) on an r:t beam splitter with coefficient $t = \sqrt{(1-p)^{N_1}}$ and $r = \sqrt{1-t^2}$. For a fixed N_1 , the action of the beam splitter on the two-mode state can be implemented through the bimodal operator [38] $B = \exp(\theta(a_1^\dagger a_2 - a_1 a_2^\dagger))$, where a_i is the annihilation operator in mode i and where $\theta = \text{atan}(r/t)$. We get the final output density matrix of our state by tracing on mode 2 and averaging

the contributions of each possible storage time:

$$\rho_{1,p} = \frac{\sum_{N_1} \text{Tr}_2[B(N_1)(\rho_{\text{in}} \otimes \rho_0)B^\dagger(N_1)]}{N_{\text{Imax}} - N_{\text{Imin}} + 1}. \quad (3)$$

The next step is to model the mixing between the stored single photon (density matrix $\rho_{1,p}$) with a photon that just arrived in the QMC (density matrix ρ_{in}) on a 50:50 beam splitter (the system $\lambda/4 + \text{PBS}$ is equivalent to a 50:50 beam splitter). One of the output states of the beam splitter, mode 2, for instance, is then measured with homodyne detection, and CSS generation is heralded when the measurement satisfies $|x_2| < \epsilon$ (with $\epsilon = 0.2$ in the experiment). This condition corresponds to the projector Π_2^ϵ , with $\langle m | \Pi_2^\epsilon | n \rangle = \int_{|x_2| < \epsilon} \langle m | x_2 \rangle \langle x_2 | n \rangle dx_2$. The CSS generated in the cavity is then obtained after tracing on mode 2 and normalization:

$$\rho_{\text{CSS}} = \mathcal{N} \text{Tr}_2[\Pi_2^\epsilon B_{50:50}(\rho_{\text{in}} \otimes \rho_{1,p})B_{50:50}^\dagger]. \quad (4)$$

The CSS is then stored N_{CSS} round trips in the QMC. The losses induced by this storage are calculated in the same way as that for the storage of the first single photon:

$$\rho_{\text{CSS},p} = \text{Tr}_2[B(N_{\text{CSS}})(\rho_{\text{CSS}} \otimes \rho_0)B^\dagger(N_{\text{CSS}})]. \quad (5)$$

We also checked the effect of our phase uncertainty [estimated to ± 12 degrees from the variance between the data and the fit of Fig. 4(d)] and it lowers at most the final fidelity of 2.5%. This lowering was numerically calculated by drawing quadratures numerically with an error on the phase which has a 12° standard deviation.

-
- [1] T. C. Ralph, A. Gilchrist, G. J. Milburn, W. J. Munro, and S. Glancy, Quantum computation with optical coherent states, *Phys. Rev. A* **68**, 042319 (2003).
 - [2] A. P. Lund, T. C. Ralph, and H. L. Haselgrove, Fault-tolerant Linear Optical Quantum Computing with Small-Amplitude Coherent States, *Phys. Rev. Lett.* **100**, 030503 (2008).
 - [3] H.-L. Yin and Z.-B. Chen, Coherent-state-based twin-field quantum key distribution, *Sci. Rep.* **9**, 1 (2019).
 - [4] H. Le Jeannic, A. Cavaillès, J. Raskop, K. Huang, and J. Laurat, Remote preparation of continuous-variable qubits using loss-tolerant hybrid entanglement of light, *Optica* **5**, 1012 (2018).
 - [5] J. Etesse, B. Kanseri, and R. Tualle-Brouri, Iterative tailoring of optical quantum states with homodyne measurements, *Opt. Express* **22**, 30357 (2014).
 - [6] T. Douce, D. Markham, E. Kashefi, P. van Loock, and G. Ferrini, Probabilistic fault-tolerant universal quantum computation and sampling problems in continuous variables, *Phys. Rev. A* **99**, 012344 (2019).
 - [7] H. M. Vasconcelos, L. Sanz, and S. Glancy, All-optical generation of states for “Encoding a qubit in an oscillator”, *Opt. Lett.* **35**, 3261 (2010).
 - [8] D. J. Weigand and B. M. Terhal, Generating grid states from Schrödinger-cat states without postselection, *Phys. Rev. A* **97**, 022341 (2018).
 - [9] J. Etesse, R. Blandino, B. Kanseri, and R. Tualle-Brouri, Proposal for a loophole-free violation of Bell’s inequalities with a set of single photons and homodyne measurements, *New J. Phys.* **16**, 053001 (2014).
 - [10] J. Joo, W. J. Munro, and T. P. Spiller, Quantum Metrology With Entangled Coherent States, *Phys. Rev. Lett.* **107**, 083601 (2011).
 - [11] J. P. Dowling, Quantum optical metrology—the lowdown on high-N00N states, *Contemp. Phys.* **49**, 125 (2008).
 - [12] H. Kwon, K. C. Tan, T. Volkoff, and H. Jeong, Nonclassicality as a Quantifiable Resource for Quantum Metrology, *Phys. Rev. Lett.* **122**, 040503 (2019).
 - [13] B. Yurke and D. Stoler, Generating Quantum Mechanical Superpositions of Macroscopically Distinguishable States Via Amplitude Dispersion, *Phys. Rev. Lett.* **57**, 13 (1986).
 - [14] A. Ourjoumtsev, H. Jeong, R. Tualle-Brouri, and P. Grangier, Generation of optical ‘Schrödinger cats’ from photon number states, *Nature (London)* **448**, 784 (2007).
 - [15] D. V. Sychev, A. E. Ulanov, A. A. Pushkina, M. W. Richards, I. A. Fedorov, and A. I. Lvovsky, Enlargement of optical Schrödinger’s cat states, *Nat. Photonics* **11**, 379 (2017).
 - [16] T. Gerrits, S. Glancy, T. S. Clement, B. Calkins, A. E. Lita, A. J. Miller, A. L. Migdall, S. W. Nam, R. P. Mirin, and E. Knill, Generation of optical coherent-state superpositions by number-resolved photon subtraction from the squeezed vacuum, *Phys. Rev. A* **82**, 031802(R) (2010).
 - [17] M. Yukawa, K. Miyata, T. Mizuta, H. Yonezawa, P. Marek, R. Filip, and A. Furusawa, Generating superposition of up-to three

- photons for continuous variable quantum information processing, *Opt. Express* **21**, 5529 (2013).
- [18] K. Huang, H. Le Jeannic, J. Ruauudel, V. B. Verma, M. D. Shaw, F. Marsili, S. W. Nam, E. Wu, H. Zeng, Y.-C. Jeong, R. Filip, O. Morin, and J. Laurat, Optical Synthesis of Large-amplitude Squeezed Coherent-state Superpositions with Minimal Resources, *Phys. Rev. Lett.* **115**, 023602 (2015).
- [19] J. Etesse, M. Bouillard, B. Kanseri, and R. Tualle-Brouri, Experimental Generation of Squeezed cat States with an Operation Allowing Iterative Growth, *Phys. Rev. Lett.* **114**, 193602 (2015).
- [20] S. Deleglise, I. Dotsenko, C. Sayrin, J. Bernu, M. Brune, J.-M. Raimond, and S. Haroche, Reconstruction of non-classical cavity field states with snapshots of their decoherence, *Nature (London)* **455**, 510 (2008).
- [21] B. Vlastakis, G. Kirchmair, Z. Leghtas, S. E. Nigg, L. Frunzio, S. M. Girvin, M. Mirrahimi, M. H. Devoret, and R. J. Schoelkopf, Deterministically encoding quantum information using 100-photon Schrödinger cat states, *Science* **342**, 607 (2013).
- [22] B. Hacker, S. Welte, S. Daiss, A. Shaukat, S. Ritter, L. Li, and G. Rempe, Deterministic creation of entangled atom–light Schrödinger-cat states, *Nat. Photon.* **13**, 110 (2019).
- [23] M. Lewenstein, M. Ciappina, E. Pisanty, J. Rivera-Dean, P. Stammer, T. Lamprou, and P. Tzallas, Generation of optical Schrödinger cat states in intense laser–matter interactions, *Nat. Phys.* **17**, 1104 (2021).
- [24] A. P. Lund, H. Jeong, T. C. Ralph, and M. S. Kim, Conditional production of superpositions of coherent states with inefficient photon detection, *Phys. Rev. A* **70**, 020101(R) (2004).
- [25] A. Laghaout, J. S. Neergaard-Nielsen, I. Rigas, C. Kragh, A. Tipsmark, and U. L. Andersen, Amplification of realistic Schrödinger-cat-state-like states by homodyne heralding, *Phys. Rev. A* **87**, 043826 (2013).
- [26] J.-i. Yoshikawa, K. Makino, S. Kurata, P. van Loock, and A. Furusawa, Creation, Storage, and On-demand Release of Optical Quantum States with a Negative Wigner Function, *Phys. Rev. X* **3**, 041028 (2013).
- [27] K. Makino, Y. Hashimoto, J.-I. Yoshikawa, H. Ohdan, T. Toyama, P. van Loock, and A. Furusawa, Synchronization of optical photons for quantum information processing, *Sci. Adv.* **2**, e1501772 (2016).
- [28] S. Takeda, K. Takase, and A. Furusawa, On-demand photonic entanglement synthesizer, *Sci. Adv.* **5**, eaaw4530 (2019).
- [29] M. Bouillard, G. Boucher, J. Ferrer Ortas, B. Pointard, and R. Tualle-Brouri, Quantum Storage of Single-photon and Two-photon Fock States with an All-optical Quantum Memory, *Phys. Rev. Lett.* **122**, 210501 (2019).
- [30] B. Kanseri, M. Bouillard, and R. Tualle-Brouri, Efficient frequency doubling of femtosecond pulses with BIBO in an external synchronized cavity, *Opt. Commun.* **380**, 148 (2016).
- [31] M. Bouillard, G. Boucher, J. F. Ortas, B. Kanseri, and R. Tualle-Brouri, High production rate of single-photon and two-photon Fock states for quantum state engineering, *Opt. Express* **27**, 3113 (2019).
- [32] D. R. Herriott and H. J. Schulte, Folded optical delay lines, *Appl. Opt.* **4**, 883 (1965).
- [33] H. Hansen, T. Aichele, C. Hettich, P. Lodahl, A. Lvovsky, J. Mlynek, and S. Schiller, Ultrasensitive pulsed, balanced homodyne detector: Application to time-domain quantum measurements, *Opt. Lett.* **26**, 1714 (2001).
- [34] A. I. Lvovsky, Iterative maximum-likelihood reconstruction in quantum homodyne tomography, *J. Opt. B: Quantum Semiclassical Opt.* **6**, S556 (2004).
- [35] J. Řeháček, Z. Hradil, E. Knill, and A. I. Lvovsky, Diluted maximum-likelihood algorithm for quantum tomography, *Phys. Rev. A* **75**, 042108 (2007).
- [36] U. Leonhardt, *Measuring the Quantum State of Light* (Cambridge University Press, Cambridge, UK, 1997), Vol. 22.
- [37] M. Cooper, L. J. Wright, C. Söller, and B. J. Smith, Experimental generation of multi-photon fock states, *Opt. Express* **21**, 5309 (2013).
- [38] B. Yurke, S. L. McCall, and J. R. Klauder, SU(2) and SU(1,1) interferometers, *Phys. Rev. A* **33**, 4033 (1986).